Magic Angles and Fractional Chern Insulators in Twisted Homobilayer Transition Metal Dichalcogenides

Nicolás Morales-Durán[*], Nemin Wei, Jingtian Shi, and Allan H. MacDonald
Department of Physics, The University of Texas at Austin, Austin, Texas 78712, USA

We explain the appearance of magic angles and fractional Chern insulators in twisted K-valley homobilayer transition metal dichalcogenides by mapping their continuum model to a Landau level problem. Our approach relies on an adiabatic approximation for the quantum mechanics of valence band holes in a layer-pseudospin field that is valid for sufficiently small twist angles and on a lowest Landau level approximation that is valid for sufficiently large twist angles. It provides a simple qualitative explanation for the nearly ideal quantum geometry of the lowest moiré miniband at particular twist angles, predicts that topological flat bands occur only when the valley-dependent moiré potential is sufficiently strong compared to the interlayer tunneling amplitude, and provides a convenient starting point for the study of interactions.

Introduction.—Recent experiments [1–5] have reported the first observations of fractional Chern insulator (FCI) states, exotic states of matter that display a fractional quantum Hall effect in the absence of a magnetic field [6]. It has been understood for some time [8–13] that FCI states do occur in artificial theoretical model systems. In this Letter, we address FCI states in the hole fluids of AA-stacked K-valley transition metal dichalcogenide (TMD) twisted homobilayers, where the effect was first observed [1,2]. Earlier theoretical work had hinted that FCI states might appear in this type of two-dimensional electron system by showing that their moiré minibands could carry Chern numbers [14,15], that the moiré band width could mysteriously vanish [16–18] near a magic twist angle, and that the bands have almost ideal quantum geometry [19] when flat [20]. There are, however, many open questions; for example, the FCI states so far appear at a few hole filling fractions and they appear over a wider regime of twist angle than theoretically expected. In this Letter, we address the most baffling question—why do the magic angles appear in the first place? Our answer points to a strategy for quantitative descriptions of these moiré FCI states.

Continuum models of TMD moirés [14,21] are expected to give an accurate description of their low-energy physics. In bilayers, the layer-dependent terms can always be expressed in terms of an effective field that acts on the layer pseudospin. For AA-stacked K-valley homobilayers [14–16] the effective field has a topologically nontrivial spatial structure with one Skyrmion for each moiré period. It is natural to suspect that there is a connection between the real space Skyrmion lattice and the momentum space Chern numbers, although it was recognized from the beginning

[14] that the correspondence is not universal. Instead the Chern number of the topmost valence moiré miniband depends on the phenomenological parameters (V_m, ψ, ω) that enter the continuum model, whose values vary from system to system [14–16,19,22,23], and can vanish even though the Skyrmion lattice is always present. Here V_m, ψ, and ω, respectively, specify the strength and shape of the moiré potentials in each layer, and the strength of interlayer tunneling.

In this Letter, we exploit an approximation to the TMD continuum model that is motivated by the presence of the Skyrmion lattice, one that maps it to holes in Landau levels subject to a periodic potential, to explain the magic angle behavior. We start by using an adiabatic approximation for the layer pseudospin to transform the continuum Hamiltonian into one for layerless holes under the effect of a periodic potential and a periodic magnetic field with a nonzero mean. By separating the effective magnetic field into average and sinusoidal contributions, we further project the problem to the lowest Landau level (LLL) induced by the average effective magnetic field, whose strength is one flux quantum per moiré unit cell. Within the LLL, both field and potential variations can be grouped into an effective potential with honeycomb lattice symmetry that is accurately characterized by a single real parameter ξ_1, whose value is determined by the continuum model parameters. We show that the magic angle behavior occurs when ξ_1 vanishes. At the magic angle, our series of transformations has mapped the bilayer Hamiltonian to the ordinary fractional quantum Hall problem, making the fractional Hall effect inevitable.

Adiabatic approximation.—We start from the continuum model Hamiltonian for TMD homobilayers [14],

$$H_{\text{TMD}} = -\frac{\hbar^2 k^2}{2m^*}\sigma_0 + \mathbf{\Delta}(\mathbf{r}) \cdot \boldsymbol{\sigma} + \Delta_0(\mathbf{r})\sigma_0, \qquad (1)$$

where $\mathbf{\Delta} = [\text{Re}\,\Delta_T, \text{Im}\,\Delta_T, (\Delta_b - \Delta_t)/2]$, Δ_T is the complex interlayer tunneling amplitude, $\Delta_0 = (\Delta_b + \Delta_t)/2$, where Δ_t and Δ_b are the potential energies in the top and bottom layers, $\boldsymbol{\sigma} = (\sigma_x, \sigma_y, \sigma_z)$ are the Pauli matrices and σ_0 the identity matrix. Equation (1) is a valley-projected single-particle Hamiltonian; the full Hilbert space includes two valleys that are related to each other by time reversal. For details on the continuum model see the Supplemental Material [24].

Next we apply a unitary transformation $U(\mathbf{r})$ that rotates $\mathbf{\Delta}(\mathbf{r})$ to the z direction at each position [28–31]

$$U^\dagger(\mathbf{r})[\mathbf{\Delta}(\mathbf{r}) \cdot \boldsymbol{\sigma}]U(\mathbf{r}) = |\mathbf{\Delta}(\mathbf{r})|\sigma_z. \qquad (2)$$

Because the transformation is position dependent, the kinetic energy term includes coupling between the up and down pseudospin sectors. Projection to the up pseudospin sector can, however, be justified when the $\mathbf{r}$ dependence is slow. After projection to the up pseudospin sector, which we will refer to as the adiabatic approximation, the matrix Hamiltonian operator reduces to a scalar. Because of the real space Berry phases associated with the Skyrmion lattice [14] in the pseudospin field, the kinetic-energy operator gains an effective periodic magnetic field with nonzero mean. Additionally, there is a contribution from the off-diagonal part of the matrix Hamiltonian, the kinetic potential

$D = (\hbar^2/8m^*)\sum_{i=x,y}[\partial_i \mathbf{n}]^2$, which is the local increase in kinetic energy due to the position-dependence of the layer spinor, with $\mathbf{n}(\mathbf{r}) = \mathbf{\Delta}(\mathbf{r})/|\mathbf{\Delta}(\mathbf{r})|$. The effective Zeeman energy is $\tilde{\Delta} = |\mathbf{\Delta}| + \Delta_0$, yielding [32–36]

$$H = -\frac{1}{2m^*}[\hbar \mathbf{k} + e\tilde{\mathbf{A}}(\mathbf{r})]^2 - D(\mathbf{r}) + \tilde{\Delta}(\mathbf{r}). \qquad (3)$$

The adiabatic approximation is valid when $|\mathbf{\Delta}(\mathbf{r})| \gg \hbar^2/(m^* A_M)$, where A_M is the moiré unit cell area. The emergent magnetic field in Eq. (3) is proportional [15] to the Pontryagin index density of $\mathbf{n}(\mathbf{r})$,

$$\mathbf{B}_{\text{eff}}(\mathbf{r}) = \boldsymbol{\nabla} \times \tilde{\mathbf{A}}(\mathbf{r}) = \frac{\hbar}{2e}\mathbf{n} \cdot (\partial_x \mathbf{n} \times \partial_y \mathbf{n}), \qquad (4)$$

and therefore has one flux quantum per moiré period. In magnetic thin films with noncollinear spin textures a similar effective magnetic field is responsible for the topological Hall effect [28–31]. See Supplemental Material for details on how to obtain Eq. (3) [24].

Figure 1(a) shows the spatial dependence of the effective magnetic field for continuum model parameters corresponding to unstrained MoTe$_2$. $\mathbf{B}_{\text{eff}}$ has three sharp peaks per period centered on the m points of the Wigner-Seitz cell. We separate the effective magnetic field into an average value, $\mathbf{B}_0 = \Phi_0/A_M$, where Φ_0 is the magnetic flux quantum, and a position-dependent part, denoted by $\mathbf{B}(\mathbf{r})$, that has zero average. The corresponding vector potential can be split in a similar way so that
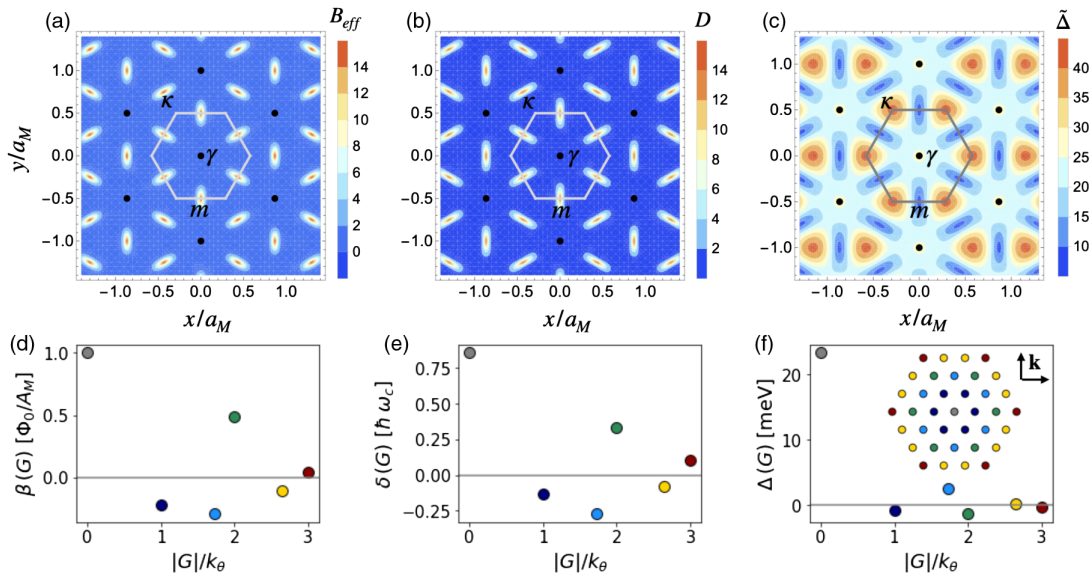
FIG. 1. Spatial distribution of the (a) effective magnetic field $\mathbf{B}_{\text{eff}}(\mathbf{r})$ generated by the layer pseudospin skyrmion in units of flux quantum per unit cell area, (b) the kinetic potential D in units of $\hbar\omega_c$, and (c) the effective Zeeman field $\tilde{\Delta}(\mathbf{r})$ in meV. Black dots indicate moiré superlattice sites. The Wigner-Seitz cell boundary is marked by solid lines and the κ, m, and γ high symmetry points that are key to magic angle behavior (see main text) are indicated. (d)–(f) The corresponding Fourier expansion coefficients. The inset in (f) shows the first six shells of reciprocal lattice vectors. The magnetic form factors have the numerical values $1, 0.163, 4 \times 10^{-3}, 7 \times 10^{-4}$, $3 \times 10^{-6}, 8 \times 10^{-8}$ for the six plotted shells. These illustrative plots are for unstrained MoTe$_2$ [14] model parameters: $V_m = 8$ meV, $\psi = 89.6°$, and $\omega = -8.5$ meV.

$$\boldsymbol{B}_{\text{eff}}(\boldsymbol{r}) = \boldsymbol{B}_0 + \boldsymbol{B}(\boldsymbol{r}) = \nabla \times \boldsymbol{A}_0 + \nabla \times \boldsymbol{A}(\boldsymbol{r}); \qquad (5)$$

$\boldsymbol{A}_0$ is a linear function of position while $\boldsymbol{A}(\boldsymbol{r})$ has the moiré superlattice periodicity. The adiabatic Hamiltonian becomes

$$H = -\frac{\hbar^2}{2m^*}\left[\boldsymbol{\Pi} + \frac{e}{\hbar}\boldsymbol{A}(\boldsymbol{r})\right]^2 - D(\boldsymbol{r}) + \tilde{\Delta}(\boldsymbol{r}), \qquad (6)$$

where we have defined $\boldsymbol{\Pi} = \boldsymbol{k} + e\boldsymbol{A}_0/\hbar$. The shape of D in Fig. 1(b) is similar to that of $\boldsymbol{B}_{\text{eff}}$. Both quantities are peaked near the m points of the Wigner-Seitz cell, midway between the chalcogen on metal (XM) and metal on chalcogen points (MX) at the κ Wigner-Seitz cell corners. The spatial distribution of the effective Zeeman field $\tilde{\Delta}$ is shown in Fig. 1(c). The peaks at κ are due to large potential difference between layers, whereas those at γ are due to peaks in interlayer tunneling at metal on metal (MM) positions. As we will explain, the magic angle behavior is intimately related to the spatial pattern of the effective Zeeman field.

Because $\boldsymbol{B}_{\text{eff}}$, D and $\tilde{\Delta}$ are periodic functions, they have the moiré lattice Fourier expansion

$$\boldsymbol{B}_{\text{eff}}(\boldsymbol{r}) = \sum_{\boldsymbol{G}}\beta(\boldsymbol{G})e^{i\boldsymbol{G}\cdot\boldsymbol{r}}, \qquad (7)$$

$$D(\boldsymbol{r}) = \sum_{\boldsymbol{G}}\delta(\boldsymbol{G})e^{i\boldsymbol{G}\cdot\boldsymbol{r}}, \qquad (8)$$

$$\tilde{\Delta}(\boldsymbol{r}) = \sum_{\boldsymbol{G}}\Delta(\boldsymbol{G})e^{i\boldsymbol{G}\cdot\boldsymbol{r}}, \qquad (9)$$

where $\boldsymbol{G}$ are reciprocal lattice vectors. Since these three functions have C_6 rotational symmetry, the Fourier coefficients are identical within reciprocal lattice vector shells and real. Figures 1(d)–1(f) show the Fourier expansion coefficients for the first six shells of $\boldsymbol{B}_{\text{eff}}$, $D(\boldsymbol{r})$, and $\tilde{\Delta}$, respectively. The kinetic momentum term in Eq. (6) can then be expressed in terms of the Landau level ladder operators a and $a^\dagger$ and the complex vector potential $A_\pm = A_x \pm iA_y$, see Ref. [24]. Using $A(\boldsymbol{k}) = i\boldsymbol{k} \times \boldsymbol{B}(\boldsymbol{k})/|\boldsymbol{k}|^2$, we find that $A_\pm(\boldsymbol{G}) = \sum_{\boldsymbol{G}}\alpha_\pm(\boldsymbol{G})e^{i\boldsymbol{G}\cdot\boldsymbol{r}}$, with the Fourier coefficients given by

$$\alpha_\pm(\boldsymbol{G}) = \frac{\pm G_x + iG_y}{|\boldsymbol{G}|^2}\beta(\boldsymbol{G}). \qquad (10)$$

It follows that the Landau level representation of the adiabatic Hamiltonian is

$$H = -\hbar\omega_c\left(a^\dagger a + \frac{1}{2}\right)$$
$$+ \frac{ie\hbar}{\sqrt{2}m^*\ell}\sum_{\boldsymbol{G}}(a\alpha_+(\boldsymbol{G}) - a^\dagger\alpha_-(\boldsymbol{G}))e^{i\boldsymbol{G}\cdot\boldsymbol{r}}$$
$$- \frac{e^2}{2m^*}\sum_{\boldsymbol{G},\boldsymbol{G}'}\alpha_+(\boldsymbol{G})\alpha_-(\boldsymbol{G}')e^{i(\boldsymbol{G}+\boldsymbol{G}')\cdot\boldsymbol{r}}$$
$$- \sum_{\boldsymbol{G}}\delta(\boldsymbol{G})e^{i\boldsymbol{G}\cdot\boldsymbol{r}} + \sum_{\boldsymbol{G}}\Delta(\boldsymbol{G})e^{i\boldsymbol{G}\cdot\boldsymbol{r}}. \qquad (11)$$

In Eq. (11) $\alpha_\pm$ has been expressed in units of Φ_0/A_M, $\hbar\omega_c = 2\pi\hbar^2/(m^*A_M) \approx 2.1(\theta[\text{deg}])^2$ meV is the effective Landau level splitting, and θ is the twist angle. The numerical value here is estimated for $MoTe_2$, but similar values will hold in WSe_2. At typical twist angles the Landau level splitting is large enough with respect to Landau level mixing to justify projection of the interacting electron Hamiltonian onto the lowest effective Landau level [see Fig. 3(c) below].

Lowest Landau level projection.—Given the periodic effective fields, it is convenient to examine the lowest Landau level (LLL) projection of Eq. (11) in a representation of Landau gauge guiding center states $|X\rangle$. The Hamiltonian can be mapped to one for LLL holes experiencing a potential [37,38] with moiré periodicity:

$$\langle X'|H|X\rangle = -\frac{\hbar\omega_c}{2}\delta_{X',X} + \sum_{m,\boldsymbol{G}_m}\xi_m\langle X'|e^{i\boldsymbol{G}_m\cdot\boldsymbol{r}}|X\rangle, \qquad (12)$$

where m is a reciprocal lattice vector shell label, $\boldsymbol{G}_m$ belongs to shell m, and

$$\langle X'|e^{i\boldsymbol{G}\cdot\boldsymbol{r}}|X\rangle = e^{-|\boldsymbol{G}|^2\ell^2/4}e^{\frac{i}{2}G_x(X+X')}\delta_{X',X+G_y\ell^2}, \qquad (13)$$

where ℓ is the effective magnetic length ($2\pi\ell^2 B_0 = \Phi_0$). In Eq. (12) the effective periodic potential has contributions from both kinetic and potential terms [24]:

$$\xi_m = -\frac{\hbar e}{2m^*}\alpha_+(\boldsymbol{G}_m)G_{m-} - \delta(\boldsymbol{G}_m) + \Delta(\boldsymbol{G}_m)$$
$$- \frac{e^2}{2m^*}\sum_{\boldsymbol{G}'}\alpha_+(\boldsymbol{G}_m - \boldsymbol{G}')\alpha_-(\boldsymbol{G}'). \qquad (14)$$

Because the ξ_0 contribution yields only a constant energy and the magnetic form factor $e^{-|\boldsymbol{G}|^2\ell^2/4}$ suppresses contributions from higher shells, the LLL physics is controlled almost entirely by the Fourier coefficient corresponding to the first shell of reciprocal lattice vectors, ξ_1. The LLL electronic structure can be calculated analytically when only ξ_1 is nonzero and yields a band width proportional to $|\xi_1|$ [24]. We will now demonstrate that magic angle behavior occurs when $\xi_1 = 0$. When this condition is satisfied, the transformed Hamiltonian is equivalent to that

of interacting holes in an ordinary Landau level and states in the same universality class as the Laughlin state are expected for fillings $1/m$.

Magic angles.—Using Eq. (10) and keeping only the $m = 1$ contribution, the coefficient in Eq. (14) simplifies to

$$\xi_1 = \hbar\omega_c\left(\frac{|\bar{\beta}_1|}{2} - \frac{\sqrt{3}\bar{\beta}_1^2}{8\pi} - \bar{\delta}_1\right) + \Delta_1, \qquad (15)$$

where $\bar{\beta}_1$ and $\bar{\delta}_1$ are dimensionless [24]. Figures 2(a)–2(c) show the dependence of Δ_1, δ_1 and β_1 on the shape parameter ψ and on the ratio V_m/ω. The coefficient of $\hbar\omega_c$ in Eq. (15) is always positive because the pseudospin field direction changes most rapidly near the m-points in the unit cell [24]. Since $\hbar\omega_c \propto \theta^2$ and Δ_1 is independent of θ, it follows that ξ_1 can cross zero as a function of twist angle only if Δ_1 is negative. Because interlayer tunneling is strong near the γ points in the moiré cell, it makes a positive contribution to Δ_1. In order for Δ_1 to be negative, there must be a large contribution to Δ from the moiré modulation potential at the κ points. These observations explain the dependence of Δ_1 on V_m/w in Fig. 2(c), from which we conclude that magic angles will normally appear for $V_m/w \gtrsim 0.6$. As seen in Fig. 2(d), Δ_1 changes sign at approximately the same value of ψ as the Chern number of the topmost moiré band changes from zero to one [15,24], illustrating that the shape of the Skyrmion texture is critical for the formation of topological bands in TMD homobilayers.

In Fig. 3(a) we plot as an example the evolution of ξ_1 with twist angle for a model [14] of unstrained MoTe$_2$ bilayers. In Fig. 3(b) the band width of the adiabatic

approximation effective LLL calculated directly from Eq. (12) is compared to the corresponding continuum model band width, showing good agreement for the location of the magic angles. When the continuum model is improved by accounting for structural relaxation [22], the resulting magic angle is closer to experimental values [1,2], $\theta \approx 3.75°$. The vanishing of ξ_1 indicates a local cancellation between the zero-point kinetic energy of the effective magnetic field and a Zeeman energy given by the periodic potential. This effect is reminiscent of a similar cancellation that occurs for arbitrary magnetic field distributions in two-dimensional electron gases when the ratio of the Zeeman spin splitting to $\hbar\omega_c$ equals 1, as first observed by Aharonov and Casher [39]. In the Supplemental Material [24] we give an alternative version of the magic angle argument that is related to the Aharonov-Casher cancellation [39,40]. It implies that ideal quantum geometry develops when the zero-point kinetic energy cancels identically with the Zeeman energy and that our criterion for ideal flat Chern band formation is accurate, even when LL mixing is not negligible.

Finally, we note that the band width of the LLL effective model goes to a finite value $\propto |\Delta_1|$ in the limit $\theta \to 0$, while for the continuum model the band width vanishes in the same limit, emphasizing that Landau level mixing is essential at very small twist angles. Figure 3(c) shows the effective LL splitting $\hbar\omega_c$ and the energy scale of LL mixing with the $n = 1$ LL, η_1, as a function of twist angle.
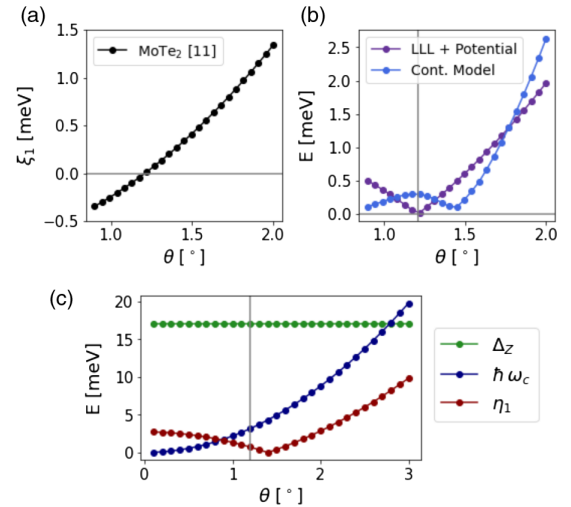
FIG. 3. (a) First Fourier coefficient of the effective periodic potential ξ_1 as a function of twist angle. (b) Bandwidth of the topmost moiré valence band from the continuum model and from our effective LLL in a periodic potential model as a function of twist angle. (c) Comparison, as a function of twist angle, between the effective Zeeman splitting Δ_Z, the effective Landau level splitting $\hbar\omega_c$, and the $n = 1$ LL mixing scale $\eta_1 = 6|\xi_1^{(1,0)}|\sqrt{2\pi}\exp(-\pi/\sqrt{3})/3^{1/4}$ [24]. The vertical line indicates the magic angle ($\xi_1 = 0$). These results are for unstrained MoTe$_2$ [14]: $V_m = 8$ meV, $\psi = 89.6°$, $\omega = -8.5$ meV.

FIG. 2. Dependence of the first-shell Fourier coefficients (a) β_1, (b) δ_1, and (c) Δ_1, on the continuum model parameter ψ and V_m/ω, the ratio of the potential and tunneling moiré modulation strengths. The units are the same as in Fig. 1. (d) Chern number of the topmost moiré band from the continuum model as a function of ψ and V_m/ω at $\theta = 2.5°$. The regions with $C_K = \pm 1$ coincide with region where $\Delta_1 < 0$.

Figure 3(c) also shows a lower bound for the effective Zeeman splitting $\Delta_Z = 2\omega$, that provides an estimation of the range of twist angles where the adiabatic approximation holds.

Discussion.—In this Letter, we have presented an analysis of K-valley twisted TMD homobilayers that is motivated by the presence [14,15] of skyrmions in the layer pseudospin field of their continuum model Hamiltonians. In an adiabatic approximation, the skyrmions give rise to a spatially periodic effective magnetic field in the valley projected Hamiltonian with one flux quantum per unit cell and a spacing between Landau levels that grows like the square of the twist angle. We show by explicit calculation that the appearance of simultaneous band width minima and nearly ideal quantum geometry [16–19], thought to be associated with the recently observed FCI [1–5] states, occurs when the effective periodic potential within the lowest effective Landau level vanishes. The transformation to a Landau level representation explains that the trace condition is almost satisfied near certain twist angles because the moiré bands inherit the ideal quantum geometry of the LLL. It also brings the knowledge gained from decades of studies of the conventional fractional quantum Hall effect to bear on the moiré FCI problem. For example, the fractional charge gaps of moiré FCI states in the absence of disorder should be $\sim 0.1 e^2/\epsilon_{\mathrm{hBN}}\ell \sim 0.25 e^2/\epsilon_{\mathrm{hBN}}\sqrt{A_M} \sim 10$ meV.

Our approach allows external magnetic fields, which are important for the Streda formula identification [1,2] of the fractional Chern insulator states, to be easily incorporated in the theory, simply by adding an external potential contribution to the average field $\boldsymbol{B}_0$. The external field will add to the Landau level degeneracy in one valley and decrease the Landau level degeneracy in the other valley, and add a preference for states that are valley polarized in the sense that aligns the orbital magnetism with the magnetic field. At a given effective Landau level filling factor, increasing the effective magnetic field will increase the interaction energy scale $e^2/\epsilon\ell$, allowing interactions to compete more strongly against effective magnetic fields. The Landau level approach to topological moiré TMDs introduced here also simplifies the treatment of the competition between interactions and both periodic and random disorder potentials. In general both periodic and random potentials will give the Landau levels a finite energy width, which will compete with the electron-electron interactions to determine the ground state at a particular band filling ν. This competition likely explains why FCI ground states are measured only at some filling factors.

It is interesting to speculate on what new frontiers in quantum Hall physics might follow from the observation of FCI states in K-valley twisted TMD homobilayers. For instance, it is natural to expect the competition between density-wave and incompressible states that is prominent in higher Landau levels [41–44] to be altered. Most

intriguingly, the effective magnetic field helps decrease magnetic lengths and increase interaction strengths beyond what is otherwise achievable. When combined with the possibility of exposing these two-dimensional electron systems to scanning probes by eliminating boron nitride encapsulation, this advance brings the prospects for manipulation of fractionalized quasiparticles much closer to reality. We leave all these interesting directions for future work.

*na.morales92@utexas.edu

[1] J. Cai, E. Anderson, C. Wang, X. Zhang, X. Liu, W. Holtzmann, Y. Zhang, F. Fan, T. Taniguchi, K. Watanabe, Y. Ran, T. Cao, L. Fu, D. Xiao, W. Yao, and X. Xu, Signatures of fractional quantum anomalous Hall states in twisted MoTe$_2$, Nature (London) **622**, 63 (2023).

[2] Y. Zeng, Z. Xia, K. Kang, J. Zhu, P. Knüppel, C. Vaswani, K. Watanabe, T. Taniguchi, K. F. Mak, and J. Shan, Thermodynamic evidence of fractional Chern insulator in moiré MoTe$_2$, Nature (London) **622**, 69 (2023).

[3] H. Park, J. Cai, E. Anderson, Y. Zhang, J. Zhu, X. Liu, C. Wang, W. Holtzmann, C. Hu, Z. Liu, T. Taniguchi, K. Watanabe, J.-H. Chu, T. Cao, L. Fu, W. Yao, C.-Z. Chang, D. Cobden, D. Xiao, and X. Xu, Observation of fractionally quantized anomalous Hall effect, Nature (London) **622**, 74 (2023).

[4] F. Xu, Z. Sun, T. Jia, C. Liu, C. Xu, C. Li, Y. Gu, K. Watanabe, T. Taniguchi, B. Tong, J. Jia, Z. Shi, S. Jiang, Y. Zhang, X. Liu, and T. Li, Observation of integer and fractional quantum anomalous Hall effects in twisted bilayer MoTe$_2$, Phys. Rev. X **13**, 031037 (2023).

[5] Z. Lu, T. Han, Y. Yao, A. P. Reddy, J. Yang, J. Seo, K. Watanabe, T. Taniguchi, L. Fu, and L. Ju, Fractional quantum anomalous Hall effect in a graphene moire superlattice, arXiv:2309.17436.

[6] Recently the term fractional Chern insulator has also been used [7] to describe fractional quantum Hall states that occur in a moiré band at nonzero magnetic field. If this terminology is adopted, the zero-field states of interest here, which combine magnetism with fractionalization since they break time-reversal spontaneously, should be referred to as fractional quantum anomalous Hall states.

[7] Y. Xie, A. T. Pierce, J. M. Park, D. E. Parker, E. Khalaf, P. Ledwith, Y. Cao, S. H. Lee, S. Chen, P. R. Forrester *et al.*, Fractional Chern insulators in magic-angle twisted bilayer graphene, Nature (London) **600**, 439 (2021).

[8] E. Tang, J.-W. Mei, and X.-G. Wen, High-temperature fractional quantum Hall states, Phys. Rev. Lett. **106**, 236802 (2011).

[9] K. Sun, Z. Gu, H. Katsura, and S. Das Sarma, Nearly flatbands with nontrivial topology, Phys. Rev. Lett. **106**, 236803 (2011).

[10] T. Neupert, L. Santos, C. Chamon, and C. Mudry, Fractional quantum Hall states at zero magnetic field, Phys. Rev. Lett. **106,** 236804 (2011).

[11] N. Regnault and B. A. Bernevig, Fractional Chern insulator, Phys. Rev. X **1,** 021014 (2011).

[12] D. N. Sheng, Z.-C. Gu, K. Sun, and L. Sheng, Fractional quantum Hall effect in the absence of Landau levels, Nat. Commun. **2,** 389 (2011).

[13] S. A. Parameswaran, R. Roy, and S. L. Sondhi, Fractional Chern insulators and the W_∞ algebra, Phys. Rev. B **85,** 241308(R) (2012).

[14] F. Wu, T. Lovorn, E. Tutuc, I. Martin, and A. H. MacDonald, Topological insulators in twisted transition metal dichalcogenide homobilayers, Phys. Rev. Lett. **122,** 086402 (2019).

[15] H. Pan, F. Wu, and S. Das Sarma, Band topology, Hubbard model, Heisenberg model, and Dzyaloshinskii-Moriya interaction in twisted bilayer WSe_2, Phys. Rev. Res. **2,** 033087 (2020).

[16] T. Devakul, V. Crépel, Y. Zhang, and L. Fu, Magic in twisted transition metal dichalcogenide bilayers, Nat. Commun. **12,** 6730 (2021).

[17] H. Li, U. Kumar, K. Sun, and S.-Z. Lin, Spontaneous fractional Chern insulators in transition metal dichalcogenide moiré superlattices, Phys. Rev. Res. **3,** L032070 (2021).

[18] V. Crépel and L. Fu, Anomalous Hall metal and fractional Chern insulator in twisted transition metal dichalcogenides, Phys. Rev. B **107,** L201109 (2023).

[19] N. Morales-Durán, J. Wang, G. R. Schleder, M. Angeli, Z. Zhu, E. Kaxiras, C. Repellin, and J. Cano, Pressure-enhanced fractional Chern insulators along a magic line in moiré transition metal dichalcogenides, Phys. Rev. Res. **5,** L032022 (2023).

[20] We do not specifically address the FQAH very recently observed [5] in rhombohedral graphene stacks.

[21] F. Wu, T. Lovorn, E. Tutuc, and A. H. MacDonald, Hubbard model physics in transition metal dichalcogenide moiré bands, Phys. Rev. Lett. **121,** 026402 (2018).

[22] C. Wang, X.-W. Zhang, X. Liu, Y. He, X. Xu, Y. Ran, T. Cao, and D. Xiao, Fractional Chern insulator in twisted bilayer $MoTe_2$, Phys. Rev. Lett. **132,** 036501 (2024).

[23] A. P. Reddy, F. Alsallom, Y. Zhang, T. Devakul, and L. Fu, Fractional quantum anomalous Hall states in twisted bilayer $MoTe_2$ and WSe_2, Phys. Rev. B **108,** 085117 (2023).

[24] See Supplemental Material at http://link.aps.org/supplemental/10.1103/PhysRevLett.132.096602 for (a) details on the continuum model for homobilayer moiré TMDs, (b) the derivation of the adiabatic Hamiltonian, (c) details on the Landau level representation of the adiabatic Hamiltonian, (d) the derivation of the expression for the magic angle, and (e) calculation of the band structure for the effective LLL model in a periodic potential, which includes Refs. [25–27].

[25] R. B. Laughlin, Anomalous quantum Hall effect: An incompressible quantum fluid with fractionally charged excitations, Phys. Rev. Lett. **50,** 1395 (1983).

[26] F. H. Claro and G. H. Wannier, Magnetic subband structure of electrons in hexagonal lattices, Phys. Rev. B **19,** 6068 (1979).

[27] D. Yoshioka, Hall conductivity of two-dimensional electrons in a periodic potential, Phys. Rev. B **27,** 3637 (1983).

[28] J. Ye, Y. B. Kim, A. J. Millis, B. I. Shraiman, P. Majumdar, and Z. Tešanović, Berry phase theory of the anomalous Hall effect: Application to colossal magnetoresistance manganites, Phys. Rev. Lett. **83,** 3737 (1999).

[29] K. Ohgushi, S. Murakami, and N. Nagaosa, Spin anisotropy and quantum Hall effect in the kagomé lattice: Chiral spin state based on a ferromagnet, Phys. Rev. B **62,** R6065 (2000).

[30] K. Hamamoto, M. Ezawa, and N. Nagaosa, Quantized topological Hall effect in skyrmion crystal, Phys. Rev. B **92,** 115417 (2015).

[31] K. A. van Hoogdalem, Y. Tserkovnyak, and D. Loss, Magnetic texture-induced thermal Hall effects, Phys. Rev. B **87,** 024402 (2013).

[32] G. Volovik, Linear momentum in ferromagnets, J. Phys. C **20,** L83 (1987).

[33] P. Bruno, V. K. Dugaev, and M. Taillefumier, Topological Hall effect and Berry phase in magnetic nanostructures, Phys. Rev. Lett. **93,** 096806 (2004).

[34] N. Paul, Y. Zhang, and L. Fu, Giant proximity exchange and flat Chern band in 2D magnet-semiconductor heterostructures, Sci. Adv. **9,** eabn1401 (2023).

[35] H. Yu, M. Chen, and W. Yao, Giant magnetic field from moiré induced Berry phase in homobilayer semiconductors, Natl. Sci. Rev. **7,** 12 (2019).

[36] D. Zhai and W. Yao, Theory of tunable flux lattices in the homobilayer moiré of twisted and uniformly strained transition metal dichalcogenides, Phys. Rev. Mater. **4,** 094002 (2020).

[37] D. Pfannkuche and R. R. Gerhardts, Theory of magneto-transport in two-dimensional electron systems subjected to weak two-dimensional superlattice potentials, Phys. Rev. B **46,** 12606 (1992).

[38] A. H. MacDonald, Quantized Hall effect in a hexagonal periodic potential, Phys. Rev. B **29,** 3057 (1984).

[39] Y. Aharonov and A. Casher, Ground state of a spin-1/2 charged particle in a two-dimensional magnetic field, Phys. Rev. A **19,** 2461 (1979).

[40] V. Crépel, N. Regnault, and R. Queiroz, The chiral limits of moiré semiconductors: Origin of flat bands and topology in twisted transition metal dichalcogenides homobilayers, arXiv:2305.10477.

[41] A. A. Koulakov, M. M. Fogler, and B. I. Shklovskii, Charge density wave in two-dimensional electron liquid in weak magnetic field, Phys. Rev. Lett. **76,** 499 (1996).

[42] R. Moessner and J. T. Chalker, Exact results for interacting electrons in high Landau levels, Phys. Rev. B **54,** 5006 (1996).

[43] F. D. M. Haldane, E. H. Rezayi, and K. Yang, Spontaneous breakdown of translational symmetry in quantum Hall systems: Crystalline order in high Landau levels, Phys. Rev. Lett. **85,** 5396 (2000).

[44] N. Shibata and D. Yoshioka, Ground-state phase diagram of 2D electrons in a high Landau level: A density-matrix renormalization group study, Phys. Rev. Lett. **86,** 5755 (2001).